PAPER

Check for updates

Supramolecular cyclization of semiflexible cylindrical micelles assembled from rod-coil graft copolymers†

Liang Gao, Rui Hu, Pengfei Xu, Jiaping Lin, [ID] * Liangshun Zhang [ID] and Liquan Wang [ID] *

Uniform toroidal micelles can be constructed *via* the supramolecular cyclization of semiflexible cylindrical micelles, but revealing the conditions under which the cyclization occurs and the mechanism underlying the cyclization remains a challenge. In this study, we performed Brownian dynamics simulations of the supramolecular cyclization of semiflexible cylindrical micelles formed by rod-coil graft copolymers to obtain the cyclization conditions and understand the cyclization mechanism. It was found that the balance of the bending energy of the polymer backbones with the self-attraction energy between the pendant groups on the polymer backbones plays an important role in the cyclization process. A theoretical model based on this balance is developed to explain the cyclization mechanism, and the conditions required for realizing the supramolecular cyclization are obtained. The proposed mechanism is supported by our experimental findings regarding the supramolecular cyclization of polypeptide cylindrical micelles. The cyclization conditions and the revealed mechanism can guide further preparation of uniform toroidal micelles from semiflexible cylindrical micelles in an end-to-end closure manner.

Introduction

Block copolymers are able to spontaneously self-assemble in selective solvents into aggregates with a variety of morphologies, such as spherical micelles, cylindrical micelles, and vesicles.[1–3] Among these aggregates, toroidal micelles with a central internal pore have attracted considerable attention due to their unique annular geometry and potential applications, such as gene delivery and biomimetic model.[4–13] Toroidal micelles are usually considered to have potential in mimicking biological systems because many transmembrane proteins, such as β-barrels and α-helical bundles, have ring-like shapes and because DNA in most bacterial phages and vertebrate sperm cells is condensed into toroidal structures with an outer diameter of approximately 100 nm.[13–16]

Practically, the toroidal micelles reported to date can be created *via* two different mechanisms. In the first mechanism, toroidal micelles are spontaneously self-assembled from homogeneous solutions *via* nucleation and growth mecha-

nisms, that is, spherical micelles are first formed, then grow into small disks, and finally evolve into toroids through the perforation of the disks.[5,6,17–19] The more general mechanism is the end-to-end closure of rod-like or cylindrical micelles, as the toroidal micelles are essentially looped rod-like or cylindrical micelles.[4,10,11,20–26] The evolution from rod-like or cylindrical micelles to toroid structures, resembling the cyclization reactions of small molecules, can be regarded as supramolecular cyclization.[11] Pochan *et al.* revealed the origin of toroidal micelle formation and suggested that three requirements should be met to construct toroids from cylindrical micelles: high flexibility of cylinders, self-attraction of charged polymers in the corona of the cylinders, and extra end-capping energy originating from chain packing frustration.[4,9] Our recent experimental observations, however, seem beyond the scope of these requirements. We found that semiflexible (not highly flexible) cylindrical micelles with rigid polymer backbones arranged parallel to the long axis of the micelle can also be bent into toroids *via* end-to-end closure.[11] More interestingly, the immediate states of crescents can be stabilized in solution. The question then arises as to what are the requirements and mechanisms for the cyclization of semiflexible cylindrical micelles.

Theory and simulation, which are able to capture the essential features of experimental systems, can be applied to reveal the mechanism behind self-assembling systems.[18,19,27–32] To

Shanghai Key Laboratory of Advanced Polymeric Materials, Key Laboratory for Ultrafine Materials of Ministry of Education, School of Materials Science and Engineering, East China University of Science and Technology, Shanghai 200237, China. E-mail: jlin@ecust.edu.cn, lq_wang@ecust.edu.cn

this end, dissipative particle dynamics simulation,[18,27] self-consistent field theory,[28] and mesoscopic field-based simulation[19] have been employed to investigate the formation of toroidal micelles. For example, He and Schmid conducted a mesoscopic field-based simulation on the formation of toroidal micelles in copolymer solutions and proposed a mechanism in which toroidal micelles form by a pathway that proceeds *via* nucleation, growth, and subsequent breakup of disk-like micelles.[19] The proposed mechanism was proven by the experiments carried out by Chang *et al.*[6] and by Pochan *et al.*,[9] indicating the power of theoretical simulations.

In this work, we applied Brownian dynamics (BD) simulations to reveal the mechanism behind the cylinder-to-toroid transformation of semiflexible cylindrical micelles. Cylindrical micelles, curved cylinders, and toroidal micelles were observed during the cyclization (*i.e.*, end-to-end closure) process. The effects of the rigidity of the polymer backbones and the interaction strength between the pendant groups joined at the polymer backbones on this cyclization process were examined. Furthermore, a theoretical model based on the balance of the bending energy of the backbone with the interaction energy between pendant groups was developed to clarify the cyclization conditions. The theory can well account for the simulation results. Finally, the theory and simulation studies were compared with our experimental observations. The good agreement between them further supports the proposed cyclization mechanism and conditions.

Results and discussion

This section presents a study on the cyclization conditions and the mechanism of toroid formation from semiflexible cylindrical micelles. The cylindrical micelles are self-assembled from rod-coil graft copolymers comprising a rigid backbone with pendant groups and two flexible side chains (Fig. 1a). The architecture of the graft copolymer was chosen as R_m-g-$(C_n)_2$, where R, C, and the subscript denote the backbone, side chain, and bead number of each block, respectively. The model of the rod-coil copolymer corresponds to the molecular structure of the polypeptide-based graft copolymers used in the experiments. The amphiphilicity of the graft copolymers was realized by setting the interaction potentials as follows: the interactions between R and R beads were modeled with an attractive Lennard-Jones (LJ) potential to describe the hydrophobicity of the backbones, and the C–C interaction and R–C interaction were modeled with a purely repulsive LJ potential to describe the hydrophilicity of the side chain and the incompatibility between the backbone and the side chain, respectively. Since the pendant groups P represent the phenyl groups of the polypeptide backbones and exhibit strong nonbonding interactions such as π–π interactions, we modeled the P–P interaction as an attractive LJ potential. The selected interaction strengths are shown in section 1 of the ESI.†

The cyclization of cylindrical micelles into toroidal micelles was simulated using the following procedure (Fig. 1a). The
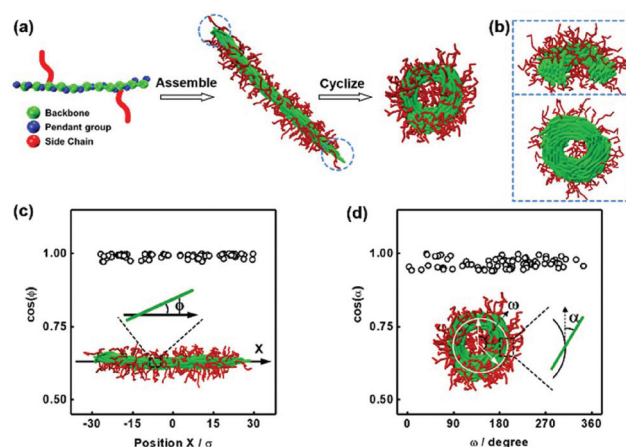

Fig. 1 Supramolecular cyclization of semiflexible cylindrical micelles. (a) Illustration of supramolecular cyclization of cylindrical micelles. The coarse-grained model of a rod-coil graft copolymer was denoted R_{12}-g-$(C_6)_2$. (b) Cross-sectional views of toroidal micelles along the diameter and the circumference. (c and d) Cosine of the orientation angle of rigid backbones along (c) the long axis of cylindrical micelles and (d) the circumference of toroidal micelles.

cylindrical micelles of the R_{12}-g-$(C_6)_2$ rod-coil graft copolymers are first formed by setting the interaction strengths $\varepsilon_{RR} = 3.5\varepsilon$ and $\varepsilon_{PP} = 1.0\varepsilon$ and the angle spring constant $k = 20\varepsilon$ (a higher k corresponds to a stronger rigidity of the polymer backbone; the other parameter settings are given in section 1 of the ESI†). In our previous work, the toroidal micelles were formed through the end-to-end closure of the cylindrical micelles of poly(γ-benzyl-L-glutamate)-g-poly(ethylene glycol) (PBLG-g-PEG) graft copolymers after adding THF into the micelle solution. THF can lead to the constriction of the phenyl groups according to the circular dichroism (CD) spectra.[11] To simulate this situation, we changed the parameter conditions, for example, increasing ε_{PP} to 5.0ε, to mimic the constriction of pendant groups. The change of interaction strength ε_{PP} can induce the bending and end-to-end closure of the cylindrical micelles into toroidal micelles (see Fig. 1a). We name such an end-to-end closure process a supramolecular cyclization of cylindrical micelles, which is akin to the cyclization of small molecules. The simulation results are consistent with our experimental observations.[11]

The structural details of the cylindrical micelles and the toroidal micelles were first examined prior to the detailed analysis of the cyclization mechanism. As shown in Fig. 1a, the cylindrical micelles consist of a core formed by the rigid backbones and a corona formed by the side chains. The rigid backbones take an ordered parallel packing in the micellar cores, while the micelle ends cannot be well covered by the side chains, resulting in the two partially exposed ends (see the marked region in Fig. 1a). The exposure of the micelle cores to the solution environment leads to extra end-capping energy. This end-capping energy can be eliminated through the end-to-end closure of the cylindrical micelles to form toroids[11] or polymerization to form nanowires in an end-to-end connection

manner.[33] Due to the short-range interaction between the two end-caps, the elimination of extra end-capping energy only occurs as the two end-cap approach, for example, at the moment of end-to-end closure during cyclization.[11] Fig. 1b shows the cross-sectional views along the diameter and the circumference of the toroidal micelle. Clearly, the rigid backbones in the core of the toroid micelles were bent. The orientations of the rigid backbones in the cores of cylindrical micelles are characterized by orientation angles ϕ of the rigid backbones (the definition of orientation angles is given in section 1.3 of the ESI†). As shown in Fig. 1c, the values of cos (ϕ) are close to 1.0, which means that the rigid backbones are approximately parallel to the long axis of the cylindrical micelles. For the toroidal micelles, the orientation angle α is defined as the angle between the direction vector of the backbones and the tangent vector of the toroids. The values of cos (α) shown in Fig. 1d suggest that the rigid backbones are parallel to each other along the contour of the toroidal micelles.

Thermodynamic conditions for supramolecular cyclization

We designed an *in silico* experiment to understand the conditions under which toroidal micelles are formed. The preassembled cylindrical micelles are formed by R_{12}-g-$(C_6)_2$ under the conditions of $\varepsilon_{PP} = 1.0\varepsilon$, $\varepsilon_{RR} = 3.5\varepsilon$, and $k = 20\varepsilon$. Then, we fixed ε_{PP} at 5.0ε and varied the values of ε_{RR} and k to examine the effects of the hydrophobicity and rigidity of the polymer backbones on the cyclization of preassembled cylindrical micelles, respectively (the other simulation parameters remain unchanged, see section 1.2 of the ESI†). We mapped out a morphology diagram in the space of ε_{RR} *versus* k to show how they influence the stability of the micelle morphologies. As shown in Fig. 2, six kinds of aggregates, namely, unimers (**U**) and cylindrical (**R**), spherical (**S**), ellipsoidal (**E**), toroidal (**T**), and curved (**C**) micelles, were observed under various parameter conditions. At lower ε_{RR} values (see the bottom region),

the backbones are not very hydrophobic, and so the cylindrical micelles disassemble into unimers (**U**). At lower k values (see the left regions), spherical (**S**) and ellipsoidal (**E**) micelles are formed from the collapse of cylindrical micelles. The toroidal (**T**) micelles are formed at only intermediate values of ε_{RR} and k, and their morphology region is surrounded by the region of curved (**C**) micelles. Higher values of ε_{RR} and k favor the stability of the cylindrical micelles.

We learn from Fig. 2 that the decrease of k (a higher k value corresponds to a more rigid backbone) can lead to the morphological transformation from cylindrical micelles to toroidal micelles for appropriate choices of interaction strength conditions (see the arrow in Fig. 2). This implies that the more rigid polymer backbones are able to resist the bending of the cylinders. According to our previous work, the interfacial energy gradually decreases during the cyclization process.[11] The interfacial energy between the micellar core and corona includes all the pairwise interaction energy among the various types of beads in the simulations, that is, **P–P**, **R–R**, **R–P**, **R–C**, **P–C**, and **C–C** interactions. To gain insights into which type of interaction is the main contributor to the bending behavior, we calculated the variations in the average energy of the various types of interactions during the cyclization process. The energy variations were calculated from the initial cylinder to the curved micelle and toroidal micelle as the backbone rigidity k decreases (see the arrow in Fig. 2). All the interaction strengths are fixed, for example, ε_{PP} and ε_{RR} are fixed at 5.0ε and 3.5ε, respectively. Fig. 3 shows the energy variations ΔE for various types of interactions. As shown in Fig. 3, with increasing k, ΔE for the **P–P** interaction gradually increases, while the ΔE for the other interactions remains nearly unchanged. Moreover, the ΔE for the **P–P** interaction is much larger than those for the other interactions, especially for
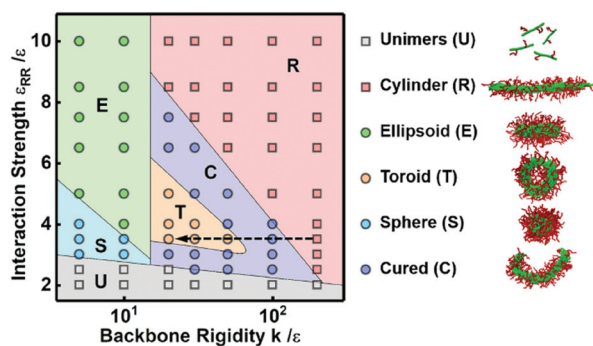

Fig. 2 Morphological diagram of aggregates transformed from preassembled cylindrical micelles. Preassembled cylindrical micelles are formed by R_{12}-g-$(C_6)_2$ under the conditions of the interaction strengths $\varepsilon_{PP} = 1.0\varepsilon$ and $\varepsilon_{RR} = 3.5\varepsilon$ and the backbone rigidity $k = 20\varepsilon$. The morphological diagram of aggregates in the space of ε_{RR} *versus* k, where ε_{PP} is fixed at 5.0ε, is shown and the other simulation parameters remain unchanged. The arrow represents the cyclization process from cylindrical micelles to curved and then toroidal micelles with the decreasing value of k.
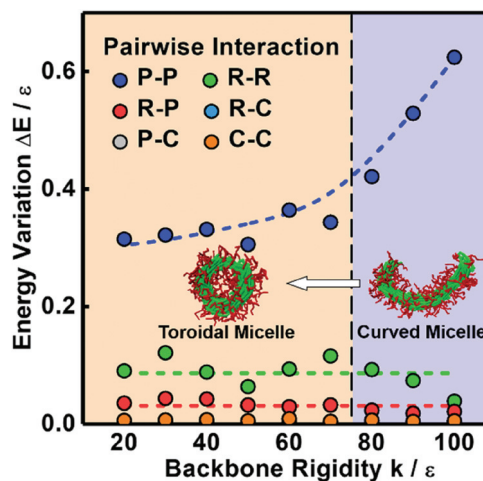
Fig. 3 Energy variations in the supramolecular cyclization process. Variations in the potential energy for all the pairwise interactions as a function of backbone rigidities k, where ε_{RR} and ε_{PP} are fixed at 3.5ε and 5.0ε, respectively. Note that the data of **P–C** and **R–C** interactions are not clearly shown in the figure due to the overlap with those of the **C–C** interaction.

more rigid backbones. This result reveals that the variation in the **P–P** interaction is the main contributor to the variation of the interfacial energy and thereby the cyclization process.

Because the **P–P** interaction plays the dominant role in determining the structural transformation from cylinders to toroids, we investigated the morphological transformation at various values of ε_{PP} between pendant groups. Representative structures are shown in Fig. 4a. With increasing ε_{PP} values, cylindrical micelles, curved cylinders, and toroidal micelles were sequentially observed. During this transformation, the cylinders are increasingly bending, and the central angle φ gradually increases (the definition of φ is illustrated in the inset of Fig. 4b). We plotted the central angle φ as a function of the ratio L/R of the arc length to the radius for the micelles, which is shown in Fig. 4b. As shown in the figure, the central angle φ is proportional to L/R, indicating that the arc lengths and structures of the micelles are nearly unchanged during the cyclization process. This inference is also demonstrated by the evidence that the circumference (63σ) of the formed toroids is very close to the initial length (69σ) of the cylindrical micelles.

To gain insights into the bending behavior, the variation in the radius R as a function of the interaction strength ε_{PP} was examined, which is shown in Fig. 4c. As the interaction strength ε_{PP} between pendant groups increases, R gradually decreases, and the central angle φ increases (according to the relation shown in Fig. 4b). This result implies that the enhancement in ε_{PP} promotes the bending of cylindrical micelles and the formation of toroids. In contrast to ε_{PP}, the

rigidity of the polymer backbones can resist the bending of the cylinders. We, therefore, plotted the variation in the radius R as a function of the value of k. As shown in Fig. 4d, as the value of k increases, R increases, and thus, φ decreases, which indicates that the cylinders bend harder as they become more rigid. In addition to the impact on the bending behavior, the rigidity of the backbone also influences the morphologies of the closed structures. The inner hole of the toroids decreases as the value of k decreases (see Fig. S6a and S6b†). This result implies that the toroids shrink as the backbones become flexible. Further decreasing the backbone rigidity ($k = 5.0\varepsilon$) leads to the collapse of toroidal micelles into spherical micelles (see Fig. S6c†).

From Fig. 3, 4c and d, we learn that the cyclization of cylindrical micelles into toroidal micelles is mainly a balance of the self-attraction between pendant groups with the rigidity of the backbone. We then develop a theoretical model to check whether these effects dominate the supramolecular cyclization. Note that the total energy $E_{cylinder}$ of the cylindrical micelle comprises the interfacial energy E_{inter}, the bending energy E_{bend} and the end-capping energy E_{end}.[11,34,35] Then, the total energy E_{curved} of the curved micelles can be written as (for the details of the theory, see section 3.1 of the ESI†)

$$
\begin{aligned}
E_{curved} &= \Delta E_{bend} + \Delta E_{inter} + E_{cylinder} \\
&\approx \Delta E_{bend}(k, \langle\theta\rangle) + \Delta E_{PP}(\varepsilon_{PP}, \langle\theta\rangle) + E_{cylinder}
\end{aligned}
\tag{1}
$$

where ΔE_{bend} and ΔE_{inter} are the variations of the bending energy and the interfacial energy, respectively. In this theory,
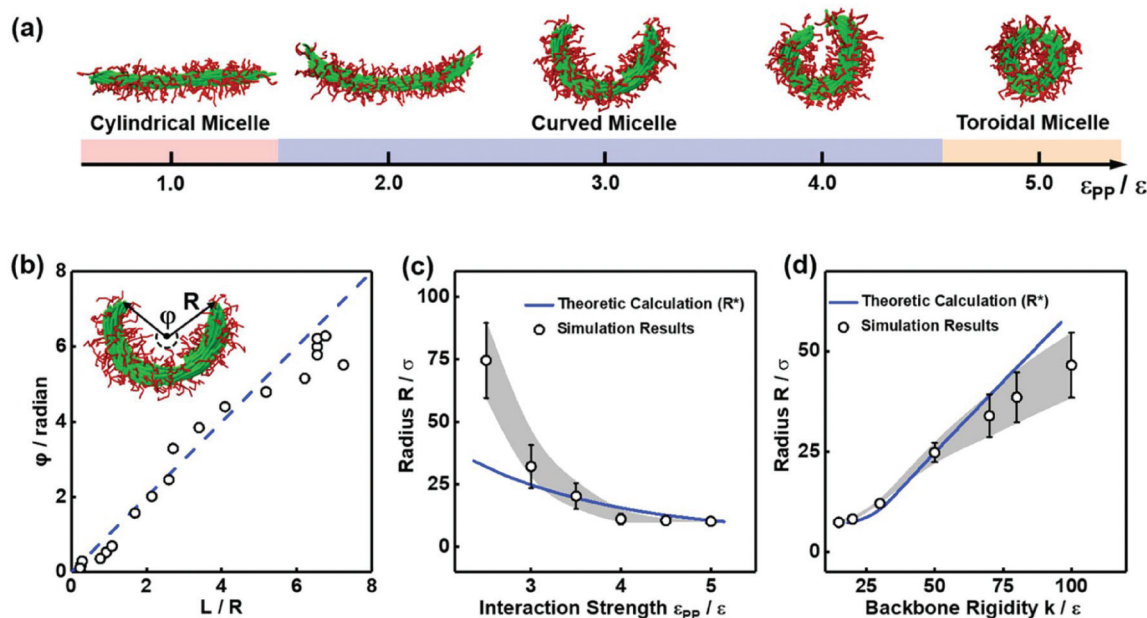

Fig. 4 Mechanism of the supramolecular cyclization. (a) Typical structures of cylindrical, curved, and toroidal micelles obtained by increasing the interaction strength ε_{PP} between pendant groups. (b) Dependence of the bend angle φ on the ratio L/R, where the blue dashed line is obtained by linear fitting (the goodness of fit is 0.9502). The inset shows the definitions of the bend angle φ of curved cylinders and the radius R of curvature. Variations in R as a function of (c) the ε_{PP} and (d) the rigidity k of the polymer backbone. The blue solid curves are the values predicted by our theory. The interaction strength ε_{RR} is fixed at 3.5ε.

ΔE_{bend} and ΔE_{inter} mainly contribute to the energy variation in the cyclization process. Here, we assumed that the end-capping energy E_{end} remains unchanged before the end-to-end closure. ΔE_{bend} and ΔE_{inter} can be estimated from the bending angle potential of the copolymer backbones $E_{\text{bend}}(k, \langle\theta\rangle)$ and the self-attraction energy E_{PP} between pendant groups, respectively, where $\langle\theta\rangle$ is the average bending angle for the rigid polymer backbone. As the minimum total energy of the curved micelle is achieved, i.e.,

$$\left.\frac{\partial E_{\text{curved}}}{\partial \langle\theta\rangle}\right|_{\langle\theta\rangle=\langle\theta\rangle^*} = 0, \quad \left.\frac{\partial^2 E_{\text{curved}}}{\partial \langle\theta\rangle^2}\right|_{\langle\theta\rangle=\langle\theta\rangle^*} > 0 \quad (2)$$

the relationship among the interaction strength ε_{PP}, the backbone rigidity k, and the radius of curvature R^* $\left(i.e., \cos\left(\frac{\langle\theta\rangle^*}{2}\right) = \frac{b}{2R^*}\right)$ satisfies

$$\varepsilon_{\text{PP}} = \frac{k(\langle\theta\rangle^* - \theta_0)}{48g_{13} - 24g_7} \quad (3)$$

Here, g_n is an exponential function with an exponent n, $g_n = c \sin\left(\frac{\langle\theta\rangle^*}{2}\right)\left(b - 2c \cos\left(\frac{\langle\theta\rangle^*}{2}\right)\right)^{-n}$, where $b = 1.5\sigma$ is the bond length of the backbone; $c = 0.75\sigma$ is the length of the bond connecting the backbone bead and pendant group; and $*$ denotes the extreme value. The variation in R^* as a function of ε_{PP} and k can be theoretically calculated using eqn (3). The calculated values are presented as blue solid lines in Fig. 4c and d. As shown in the figures, the theoretical values approach the simulation results. Although a deviation in the R^* value is found at a smaller ε_{PP} value, the difference in the central angle φ, for example, at $\varepsilon_{\text{PP}} = 2.5\varepsilon$, does not exceed 1 degree. The slight deviation between the theoretical prediction and simulation results could be attributed to the fact that the theory neglects the fluctuations of bond lengths and bond angles. Nevertheless, the good agreement between the theory and simulation results supports our proposed mechanism that the balance of the self-attraction energy between pendant groups and the bending energy of the copolymer backbones plays the dominant role in the cyclization process. Note that the formation of toroids is not to eliminate the end-cap energy only. Due to the balance of the interfacial energy to the bending energy, the curved micelles are more favorable than the straight cylinders as the solvent condition changes.

Geometric conditions for supramolecular cyclization

Apart from the above thermodynamic conditions, the cylindrical micelles must satisfy a geometric requirement for forming toroids. When the end-to-end closure of the cylinder occurs, the circumference of toroidal micelles is equal to the length L of the initial cylinder, and the diameter of the toroidal cylinder is close to the diameter D of the initial cylinder. Because the hole in the center of the toroid is a necessary geometric feature, the diameter of the toroid should be larger than the diameter of the toroidal cylinder. Thus, we can obtain geometric conditions for the end-to-end closure to form toroidal

micelles, that is, the aspect ratio L/D of the cylindrical micelles has to be larger than π ($L/D > \pi$) (for details, see section 3.2 of the ESI†).

Herein, to verify the proposed geometric conditions, the effect of the micelle size on the supramolecular cyclization of the cylindrical micelles was examined. We first obtained cylindrical micelles of various lengths from the self-assembly of three types of rod-coil graft copolymers, that is, $R_8\text{-}g\text{-}(C_6)_2$, $R_{12}\text{-}g\text{-}(C_6)_2$, and $R_{14}\text{-}g\text{-}(C_6)_2$, as shown in Fig. 5a–c. The interaction strength ε_{RR} and the backbone rigidity k were set as 3.5ε and 20ε, respectively. The simulation results indicate that the aspect ratio of the cylindrical micelles increases with the length of the polymer backbones (see the insets of Fig. 5a–c). Fig. 5g shows the distribution of the aspect ratio L/D of the pre-assembled cylindrical micelles assembled from various kinds of graft copolymers. The statistical results were obtained from more than 200 micelles from 10 groups of independent simulations. As shown in the figure, the cylindrical micelles exhibit polydisperse distributions. As the length of the rigid back-bones increases, the aspect ratio L/D gradually increases, and its distribution becomes wider. For the preassembled micelles formed by $R_8\text{-}g\text{-}(C_6)_2$ graft copolymers, the value of L/D for approximately 56% of the micelles is larger than π (as shown
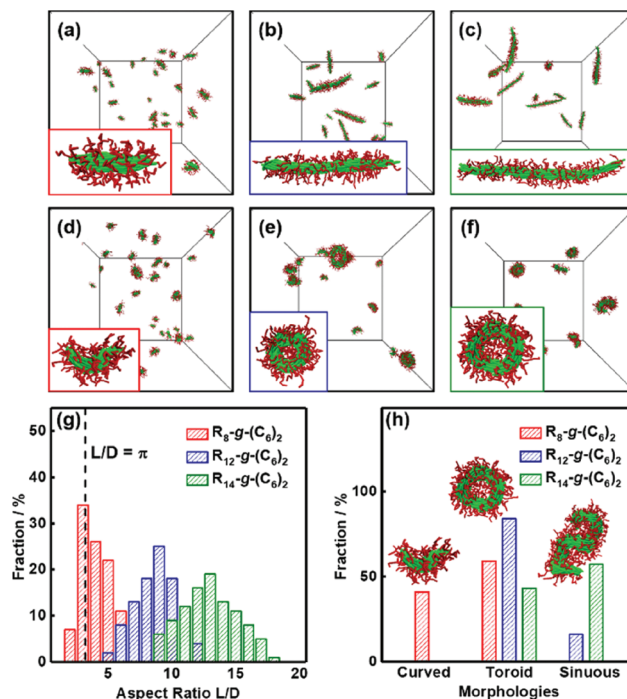

Fig. 5 Effect of micelle size on supramolecular cyclization. Simulation snapshots of semiflexible cylindrical micelles assembled from graft copolymers with architectures of (a) $R_8\text{-}g\text{-}(C_6)_2$, (b) $R_{12}\text{-}g\text{-}(C_6)_2$, and (c) $R_{14}\text{-}g\text{-}(C_6)_2$. The interaction strength ε_{RR} and the backbone rigidity k are fixed at 3.5ε and 20ε, respectively. (d–f) The aggregates transformed from the cylindrical micelles shown in (a–c), respectively, upon increasing ε_{PP} to 5.0ε. (g) Distribution of the aspect ratio L/D of the cylindrical micelles. (h) Number fraction of various morphologies (curved, toroid, and sinuous micelles) generated upon increasing ε_{PP} to 5.0ε.

by the dashed line in Fig. 5g), while the values of L/D are always larger than π for all the preassembled micelles formed by R_{12}-g-$(C_6)_2$ and R_{14}-g-$(C_6)_2$ graft copolymers.

We then changed the conditions, *i.e.*, increased ε_{PP} to 5.0ε, to realize the cyclization of three kinds of preassembled cylindrical micelles. Fig. 5d–f display the corresponding simulation snapshots of the obtained aggregates. Curved micelles with partially open ends are formed *via* the bending of the short cylindrical micelles, while the cylindrical micelles with intermediate lengths are mainly end-to-end closed into toroidal micelles (Fig. 5d and e). Moreover, the toroids with larger holes and the sinuous micelles are formed by longer cylindrical micelles (Fig. 5f). The morphologies of aggregates including toroidal, curved, and sinuous micelles coexist as shown in Fig. 5d–f due to the polydispersity of the aspect ratio of initial cylinders. Then, we analyzed the fractions of various morphologies transformed from the three groups of preassembled cylindrical micelles, respectively. The statistical results are shown in Fig. 5h. For the preassembled micelles of R_8-g-$(C_6)_2$ graft copolymers, 59% of the cylindrical micelles can cyclize to form toroidal micelles, while the remainders are bent into curved micelles (see the red columns). The fraction (59%) of toroids is close to the fraction (56%) of the preassembled cylinders that satisfy the geometric conditions of $L/D > \pi$. In addition, the graft copolymers R_6-g-$(C_6)_2$ with shorter backbones can assemble into micelles with lower L/D ($L/D < \pi$ for 95% micelles), and these micelles cannot cyclize into toroids or even bend into curved micelles (see Fig. S7†). Even if we further enhance ε_{PP} to 7.0ε, curved or toroidal micelles still cannot be observed. In contrast, 84% of the preassembled micelles formed by R_{12}-g-$(C_6)_2$ graft copolymers are cyclized into toroidal micelles (see the blue column). The fraction decreases to 43% for the cylindrical micelles of R_{14}-g-$(C_6)_2$ graft copolymers (see the green column) because the sinuous micelles are formed at significantly larger aspect ratios (see the inset in Fig. 5h). This phenomenon may be ascribed to the decreased probability of the end-to-end collision and closure for the ends of longer cylindrical micelles. The results reveal that an appropriate aspect ratio L/D is necessary to form toroidal micelles, which is in good agreement with the geometric conditions proposed based on the cyclization theory.

Comparison with experiments

In our previous work, we discovered the supramolecular cyclization of cylindrical micelles self-assembled from polypeptide-based graft copolymers PBLG-g-PEG.[11] The PBLG backbones, which take a α-helix conformation, are semiflexible, while the PEG side chains are flexible. PBLG-g-PEG can thus be modeled as a rod-coil graft copolymer. We first prepared cylindrical micelles through the self-assembly of PBLG-g-PEG and then added THF to the solution. The addition of THF results in the constriction of the phenyl groups of PBLG, which leads to the end-to-end closure of the cylindrical micelles into toroidal micelles. In this work, we analyzed previous experimental results and carried out some additional experiments. Then, we compared these experimental observations with simulation

results and explained the supramolecular cyclization behaviors of the polypeptide micelles with the proposed theory.

Thermodynamic conditions (effect of interaction strength between pendant groups). The effect of the THF content on the aggregate morphologies from the preassembled cylindrical micelles was examined.[11] Herein, we further analyzed the previous results and calculated the radius of curvature R for the aggregates formed at various THF contents, where the statistical result was obtained from more than 200 micelles. Fig. 6a shows a plot of R as a function of the THF content. As shown in the figure, the radius R gradually decreases with the increasing THF content. When the THF content is above 50.0 vol%, an end-to-end closure process occurs, and toroidal micelles are formed. The CD spectra revealed that the addition of THF can result in the constriction of the pendant groups, corresponding to the enhancement of the interaction strength ε_{PP}.[11] In the simulations, with increasing ε_{PP}, cylindrical micelles transform into curved cylinders and then toroids. The simulation results are plotted in Fig. 6 again. The dependence of the radius R on ε_{PP} shows a similar tendency to the dependence of R on the THF content in the experiments (see Fig. 6a). In addition, Fig. 6a also shows the theoretical predicated curve which is qualitatively consistent with the experimental results. Therefore, the proposed theory is applicable to describe the cyclization behaviors of polypeptide cylindrical micelles.

Geometric conditions (effect of the aspect ratio of micelles). The aspect ratio of the micelles is determined by the length of the rigid backbone, which is revealed by the simulations (see Fig. 5g). Herein, we synthesized rod-coil graft copolymers with various lengths of PBLG backbones, PBLG$_{90\,000}$-g-PEG$_{750}$, PBLG$_{120\,000}$-g-PEG$_{750}$, and PBLG$_{170\,000}$-g-PEG$_{750}$, to examine the effect of the aspect ratio on the toroid formation (the details of the synthesis and characterization of the graft copolymers are given in section 2 of the ESI†). The subscripts denote the weight-average molecular weights M_w of PBLG backbones and PEG chains, respectively. A two-step self-assembly experiment was carried out as follows. In the first step of self-assembly, 0.3 mL of deionized water (a selective solvent for PEG) was added to 2.0 mL of PBLG-g-PEG solution (THF/DMF, 1 : 1, v/v), and then the mixture solution was dialyzed against deionized water for 3 days. The cylindrical micelles can be formed by PBLG$_{90\,000}$-g-PEG$_{750}$, PBLG$_{120\,000}$-g-PEG$_{750}$, and PBLG$_{170\,000}$-g-PEG$_{750}$ in the first-step assembly. As shown in Fig. 6c, e and g, the micelle lengths for the three groups of samples are *ca.* 390 nm (aspect ratio $L/D = 0.92\pi$), *ca.* 445 nm ($L/D = 0.97\pi$), and *ca.* 550 nm ($L/D = 1.30\pi$), respectively. The aqueous solution of cylindrical micelles is stable and can be used for further cyclization. Synchrotron radiation small-angle X-ray scattering (SAXS) and wide-angle X-ray scattering (WAXS) results suggest that the PBLG backbones take an ordered packing manner in the micellar core (Fig. S11†), which is consistent with the theoretical simulations (Fig. 1).

Then, 1.2 mL of THF was added to 1.0 mL of the cylindrical micelle solutions (the resulting THF content is 54.5 vol%) to induce the cyclization reaction. Fig. 6d, f and h show the SEM
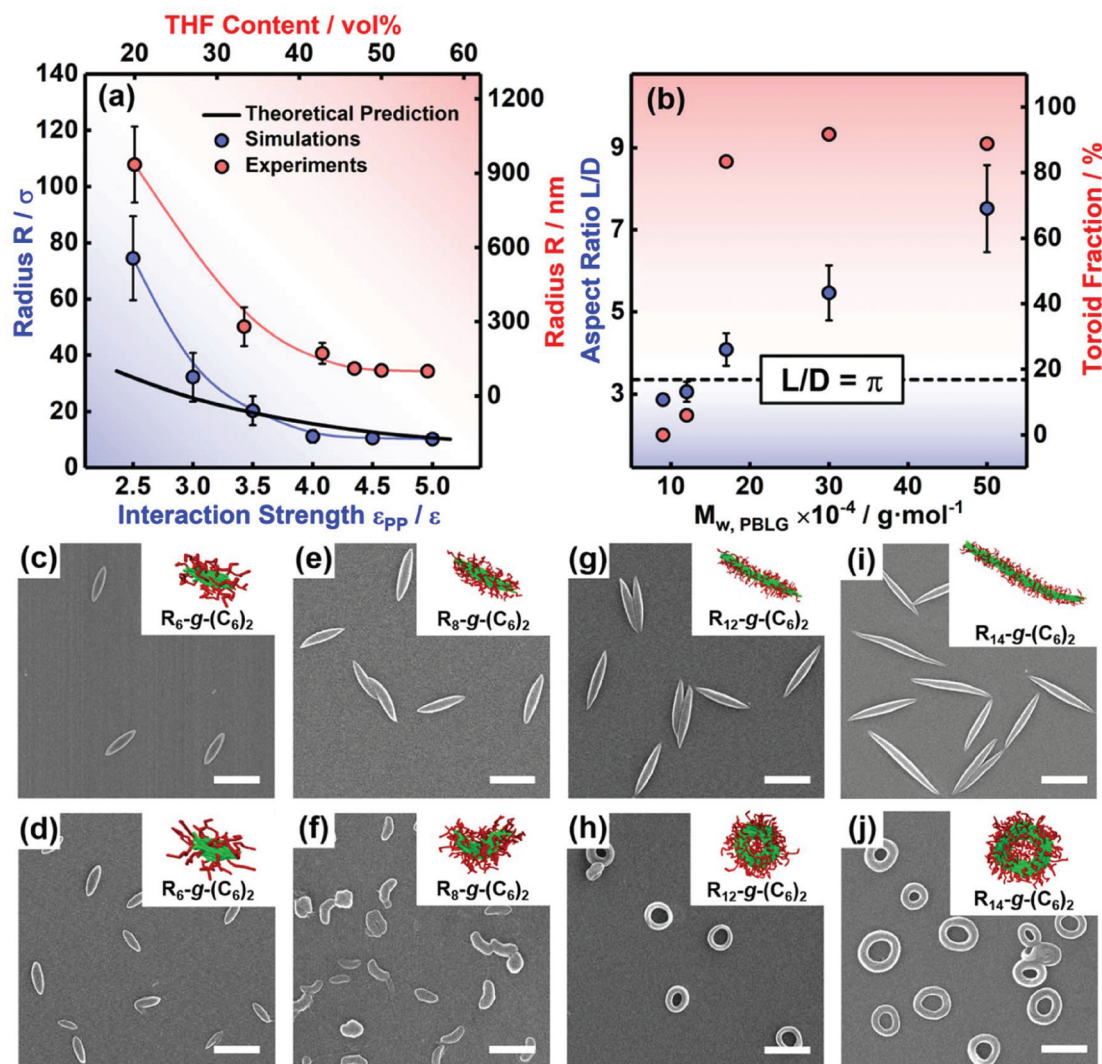
Fig. 6 Supramolecular cyclization of semiflexible cylindrical micelles assembled from PBLG-*g*-PEG graft copolymers. (a) Dependence of the curvature radius *R* on ε_{PP} and the variation in *R* as a function of THF content according to ref. 11. (b) The aspect ratio *L/D* of cylinders and the fraction of toroids for the graft copolymers with various weight-average molecular weights $M_{w,PBLG}$ of PBLG backbones. SEM images of (c, e, g and i) the cylindrical micelles obtained in the first-step assembly and (d, f, h and j) the cyclized structures from the cylindrical micelles assembled from (c and d) PBLG$_{90\,000}$-*g*-PEG, (e and f) PBLG$_{120\,000}$-*g*-PEG, (g and h) PBLG$_{170\,000}$-*g*-PEG, and (i and j) PBLG$_{500\,000}$-*g*-PEG, where (i) and (j) are reproduced with permission from ref. 11. Insets show the simulated structures of rod-coil graft copolymers with various lengths of backbones. Scale bar: 500 nm.

images of the aggregates prepared from the three groups of cylindrical micelle samples. The toroidal morphologies are also confirmed by TEM and AFM measurements (Fig. S9†). Note that the parallel packing of PBLG backbones can be maintained in the core of toroidal micelles, suggested by the synchrotron radiation SAXS and WAXS measurements (Fig. S11†). For the micelle with a lower aspect ratio (*L/D* = 0.92π), the cylindrical micelles cannot be bent into curved or toroidal micelles, but ellipsoidal structures are observed (see Fig. 6d). Even if we further increase the THF content to 75.0 vol%, (*i.e.* 3.0 mL of THF was added), curved or toroidal structures still cannot be observed (see Fig. S8†). The cylinders with a medium aspect ratio (*L/D* = 0.97π) transform into the mixture of curved micelles and ellipsoidal micelles (Fig. 6f), with only

a small fraction (6%) of cylinders forming toroids, while 83% of the longer cylinders (*L/D* = 1.30π) finally cyclize into toroids (Fig. 6h). By further increasing the M_w of PBLG backbones, cylindrical micelles with larger aspect ratios were formed, and these longer cylinders can transform into larger toroids after adding THF.[11] By further analyzing the SEM images, we found that 89% of PBLG$_{500\,000}$-*g*-PEG$_{750}$ cylindrical micelles with an aspect ratio *L/D* of 2.39π can cyclize into toroids (see Fig. 6i and j; the SEM image is reproduced from ref. 11). To verify the critical value of *L/D* for supramolecular cyclization, the value of *L/D* and the fraction of toroids after adding THF are plotted as a function of the M_w of PBLG backbones in Fig. 6b. With the increasing M_w of PBLG backbones, the *L/D* value gradually increases, and the fraction of toroids significantly increases as

the L/D value is larger than π (above the dashed line in Fig. 6b). In addition, the suitable molecular weight of PEG is necessary to guarantee that the aspect ratio of micelles can satisfy the geometric condition for cyclization (Fig. S10†). The results indicate that toroidal structures can be formed from cylinders when the geometric condition of $L/D > \pi$ is satisfactory. These experimental observations are consistent with the proposed geometric condition and simulation results (see the insets of Fig. 6c–j).

In the present work, we proposed the thermodynamic and geometric conditions for the supramolecular cyclization of semiflexible cylindrical micelles, which is far beyond our preliminary work.[11] Compared to the other toroidal micelle systems,[4,9,20–26] the contribution of the bending energy to thermodynamic equilibrium is an important feature of the supramolecular cyclization of semiflexible cylindrical micelles. We noted that the high flexibility is unnecessary, and the toroidal micelles can be formed by balancing the bending energy and the interfacial energy. Therefore, our findings could deepen the understanding of cyclization of semiflexible nanoparticles and guide the precise preparation of uniform nanotoroids.

We also note that the bending behavior of cylindrical micelles is spontaneous and symmetry breaking. The symmetry breaking in our system can be attributed to the α-helix conformation of PBLG backbones. When the phenyl groups are constricted, the twist and bend of PBLG backbones can lead to the symmetry breaking in the bending of cylindrical micelles. Similar symmetry breaking can be observed in the supramolecular helical system and Mobius strips formed by chiral block copolymers.[36–38] Additionally, although the theory neglects the fluctuations of bond lengths and bond angles and simplifies the assemblies as cylinders with a uniform diameter, the proposed theory can be applicable to describe the cyclization process of semiflexible micelles and could guide us to explore the winding and cyclization behaviors of longer fibrous structures. With an improvement of the simulation model, we will try to develop a theoretical model to self-assemble the system of different copolymers in future work.[16,39,40]

Conclusions

We applied BD simulations to investigate the supramolecular cyclization of cylindrical micelles self-assembled from rod-coil graft copolymers. The self-attraction of pendant groups is able to induce the cyclization of the cylindrical micelles. However, the rigidity of the polymer backbone has to be tuned to meet the conditions of forming toroidal micelles. When the backbone is too rigid, the self-attraction energy cannot overcome the bending energy to realize the cyclization of cylindrical micelles. In contrast, when the backbone is not rigid enough, the backbones cannot sustain the toroidal structures, and collapsed aggregates are formed. A theory based on the balance of the interfacial energy to the bending energy is developed, and the corresponding thermodynamic condition is proposed. The effect of the aspect ratio L/D of the cylindrical micelles

was examined, and it was found that the geometric condition of $L/D > \pi$ is required to form toroidal micelles. The simulation results and cyclization conditions were further verified by experiments regarding the stepwise self-assembly of PBLG-g-PEG graft copolymers. The proposed cyclization conditions and the mechanism can guide future preparation of toroids from rigid cylinders in the manner of end-to-end closure and can deepen our understanding of supramolecular cyclization.

Methods

Simulation method

Brownian dynamics (BD) is a coarse-grained mesoscopic simulation method and has been successfully used to investigate the self-assembly of copolymers.[41–45] The simulations were performed by applying the simulator, a coarse-grained molecular dynamics program based on LAMMPS. We considered the simulation system consisting of rod-coil graft copolymers in implicit solvents. In the simulation, each bead represents a cluster of atoms and is connected by the harmonic spring potential. The graft copolymer comprises a rigid backbone, multiple pendant groups, and two side chains, as shown in Fig. 1a. The junction points on the backbone were chosen randomly for grafting the coil chains. The rigidity of the backbone and the pairwise interaction were given by the angle bending potential and the Lennard-Jones (LJ) potential, respectively. The simulations were conducted in a cubic box with periodic boundary conditions, and the NVT ensemble was adopted. The temporal evolution of the beads obeys the Langevin equation, including all the potentials, the friction term, and the noise term. More than 10 micelles are formed in each simulation box, and the polydisperse distribution from 10 independent groups of simulations is shown in Fig. 5. The detailed simulation method is available in section 1.1 of the ESI.†

Parameter setting

In the first step of assembly, for the purely repulsive interactions, the interaction strengths were set as $\varepsilon_{CC} = \varepsilon_{RC} = \varepsilon_{PC} = 1.0\varepsilon$. For the short-range attractive interaction, the interaction strengths were set as $\varepsilon_{RR} = 3.5\varepsilon$, $\varepsilon_{PP} = \varepsilon_{RP} = 1.0\varepsilon$. In the cyclization stage, the addition of THF can lead to the constriction of phenyl groups.[11] To simulate this situation, we increased the attractive interaction strength ε_{PP} from 1.0ε to 5.0ε. The detailed parameter settings are given in section 1.2 of the ESI.†

Polymer synthesis

PBLG was synthesized using ring-opening polymerization of BLG-NCA initiated by anhydrous trimethylamine. PBLG-g-PEG was prepared by the ester exchange reaction of PBLG with mPEG-OH. At the end of two polymerizations, the reaction mixture was precipitated into a large volume of anhydrous methanol. The product was purified twice by repeated precipitation from a chloroform solution into a large volume of anhydrous methanol and dried under vacuum.[3,11,33] The polymer synthesis is described in detail in section 2.1 of the ESI.†

Preparation of cylindrical and toroidal micelles

In the first-step assembly, the cylindrical micelles were prepared using a dialysis method. A total of 0.3 mL of deionized water, a selective solvent for PEG, was added to 2.0 mL of polymer solution (THF/DMF, 1 : 1, v/v; the initial polymer concentration was 0.5 g L^{-1}). The solution was dialyzed against deionized water for 3 days to remove the organic solvents. In the second-step assembly, 1.2 mL of THF was added to 1.0 mL of the cylindrical micelle solution in water at 30 °C (the resulting THF content in the THF/water mixed solvent is 54.5 vol%). The solution was allowed to stir for 24 hours and then dialyzed against water to remove THF.

Characterization of assemblies

The morphologies of the aggregates were obtained using a field-emission SEM (S4800, Hitachi) operating at an accelerating voltage of 15 kV. The detailed experimental information including TEM, AFM, synchrotron radiation SAXS, and WAXS measurements is available in section 2.3 of the ESI.†

Conflicts of interest

There are no conflicts to declare.

Acknowledgements

Notes and references

1 Y. Mai and A. Eisenberg, *Chem. Soc. Rev.*, 2012, **41**, 5969–5985.
2 A. H. Gröschel and A. H. Müller, *Nanoscale*, 2015, **7**, 11841–11876.
3 C. Cai, J. Lin, Y. Lu, Q. Zhang and L. Wang, *Chem. Soc. Rev.*, 2016, **45**, 5985–6012.
4 D. J. Pochan, Z. Chen, H. Cui, K. Hales, K. Qi and K. L. Wooley, *Science*, 2004, **306**, 94–97.
5 D. Presa-Soto, G. A. Carriedo, R. de la Campa and A. Presa Soto, *Angew. Chem., Int. Ed.*, 2016, **55**, 10102–10107.
6 H. Huang, B. Chung, J. Jung, H. W. Park and T. Chang, *Angew. Chem., Int. Ed.*, 2009, **48**, 4594–4597.
7 S. Al-Rehili, K. Fhayli, M. A. Hammami, B. Moosa, S. Patil, D. Zhang, O. Alharbi, M. N. Hedhili, H. Mohwald and N. M. Khashab, *J. Am. Chem. Soc.*, 2017, **139**, 10232–10238.
8 C. Liu, G. Chen, H. Sun, J. Xu, Y. Feng, Z. Zhang, T. Wu and H. Chen, *Small*, 2011, **7**, 2721–2726.
9 H. G. Cui, Z. Y. Chen, K. L. Wooley and D. J. Pochan, *Soft Matter*, 2009, **5**, 1269–1278.
10 J. Zhu, Y. Liao and W. Jiang, *Langmuir*, 2004, **20**, 3809–3812.
11 C. Yang, L. Gao, J. Lin, L. Wang, C. Cai, Y. Wei and Z. Li, *Angew. Chem., Int. Ed.*, 2017, **56**, 5546–5550.
12 K. Zhang, H. Miao and D. Chen, *J. Am. Chem. Soc.*, 2014, **136**, 15933–15941.
13 N. V. Hud and I. D. Vilfan, *Annu. Rev. Biophys. Biomol. Struct.*, 2005, **34**, 295–318.
14 R. Golan, L. I. Pietrasanta, W. Hsieh and H. G. Hansma, *Biochemistry*, 1999, **38**, 14069–14076.
15 A. P. Rolland, *Crit. Rev. Ther. Drug Carrier Syst.*, 1998, **15**, 143–198.
16 Y. Li, K. Osada, Q. Chen, T. A. Tockary, A. Dirisala, K. M. Takeda, S. Uchida, K. Nagata, K. Itaka and K. Kataoka, *Biomacromolecules*, 2015, **16**, 2664–2671.
17 S. J. Holder and N. A. J. M. Sommerdijk, *Polym. Chem.*, 2011, **2**, 1018–1028.
18 L. Chen, T. Jiang, J. Lin and C. Cai, *Langmuir*, 2013, **29**, 8417–8426.
19 X. He and F. Schmid, *Phys. Rev. Lett.*, 2008, **100**, 137802.
20 H. Yu and W. Jiang, *Macromolecules*, 2009, **42**, 3399–3404.
21 Z. Wang, F. Sun, S. Huang and C. Yan, *J. Polym. Sci., Part B: Polym. Phys.*, 2016, **54**, 1450–1457.
22 X. Li, Y. Gao, X. Xing and G. Liu, *Macromolecules*, 2013, **46**, 7436–7442.
23 D. Podder, S. Bera, M. Debnath, T. Das and D. Haldar, *J. Mater. Chem. B*, 2017, **5**, 7583–7590.
24 J. K. Kim, E. Lee, Z. Huang and M. Lee, *J. Am. Chem. Soc.*, 2006, **128**, 14022–14023.
25 I. C. Reynhout, J. J. Cornelissen and R. J. Nolte, *J. Am. Chem. Soc.*, 2007, **129**, 2327–2332.
26 S. Yagai, Y. Goto, X. Lin, T. Karatsu, A. Kitamura, D. Kuzuhara, H. Yamada, Y. Kikkawa, A. Saeki and S. Seki, *Angew. Chem., Int. Ed.*, 2012, **51**, 6643–6647.
27 X. Li, M. Deng, Y. Liu and H. Liang, *J. Phys. Chem. B*, 2008, **112**, 14762–14765.
28 Y. Jiang, J. Zhu, W. Jiang and H. Liang, *J. Phys. Chem. B*, 2005, **109**, 21549–21555.
29 T. Skrbic, T. X. Hoang and A. Giacometti, *J. Chem. Phys.*, 2016, **145**, 084904.
30 Z. Ou and M. Muthukumar, *J. Chem. Phys.*, 2005, **123**, 074905.
31 T. X. Hoang, A. Giacometti, R. Podgornik, N. T. Nguyen, J. R. Banavar and A. Maritan, *J. Chem. Phys.*, 2014, **140**, 064902.
32 R. Cortini, B. R. Care, J. M. Victor and M. Barbi, *J. Chem. Phys.*, 2015, **142**, 105102.
33 Z. Zhuang, T. Jiang, J. Lin, L. Gao, C. Yang, L. Wang and C. Cai, *Angew. Chem., Int. Ed.*, 2016, **55**, 12522–12527.
34 S. May, Y. Bohbot and A. Ben-Shaul, *J. Phys. Chem. B*, 1997, **101**, 8648–8657.
35 M. Asgari, *Eur. Phys. J. E*, 2015, **38**, 98.
36 Z. Geng, B. Xiong, L. Wang, K. Wang, M. Ren, L. Zhang, J. Zhu and Z. Yang, *Nat. Commun.*, 2019, **10**, 4090.
37 C. Tschierske, *Angew. Chem., Int. Ed.*, 2013, **52**, 8828–8878.

38 Z. Shen, Y. Jiang, R. Wang and M. Liu, *J. Am. Chem. Soc.*, 2015, **137**, 16109–16115.

39 H. Cabral, K. Miyata, K. Osada and K. Kataoka, *Chem. Rev.*, 2018, **118**, 6844–6892.

40 P. G. Millili, J. A. Selekman, K. M. Blocker, D. A. Johnson, U. P. Naik and M. O. Sullivan, *Microsc. Res. Tech.*, 2010, **73**, 866–877.

41 G. S. Grest and K. Kremer, *Phys. Rev. A*, 1986, **33**, 3628–3631.

42 Q. Zhang, J. Lin, L. Wang and Z. Xu, *Prog. Polym. Sci.*, 2017, **75**, 1–30.

43 S. Lin, N. Numasawa, T. Nose and J. Lin, *Macromolecules*, 2007, **40**, 1684–1692.

44 M. A. Horsch, Z. Zhang and S. C. Glotzer, *Phys. Rev. Lett.*, 2005, **95**, 056105.

45 L. Gao, J. Lin, L. Zhang and L. Wang, *Nano Lett.*, 2019, **19**, 2032–2036.